Journal of Thermal Science Vol.21, No.3 (2012) 230–235

DOI: 10.1007/s11630-012-0540-7 **Article ID: 1003-2169(2012)03-0230-06**

Effects of Freestream Turbulence on Bypass Transition of Separated Boundary Layer on Low-Pressure Turbine Airfoils

Hideo Taniguchi, Hiroshi Sakai and Ken-ichi Funazaki

Department of Mechanical Systems Engineering, Faculty of Engineering, Iwate University, Morioka, Japan

This paper presents experimental studies on bypass transition of separated boundary layer on low-pressure turbine airfoils, focusing on the effects of freestream turbulence on the transition process. Hot-wire probe measurements are performed on the suction side of an airfoil in the low-pressure linear turbine cascade at several Reynolds number conditions. Freestream turbulence is enhanced by use of turbulence grid located upstream of the cascade. The results of this experimental study show that the location of boundary layer separation does not strongly depend on the freestream turbulence level. However, as the freestream turbulence level increases, the size of separation bubble becomes small and the location of turbulent transition moves upstream. The size of separation bubble becomes small as the Reynolds number increases. At low freestream turbulence intensity, the velocity fluctuation due to Kelvin-Helmholtz instability is observed clearly in the shear layer of the separation bubble. At high freestream turbulence intensity, the streak structures appear upstream of the separation location, indicating bypass transition of attached boundary layer occurs at high Reynolds number.

Keywords: Aeroengine, Low-Pressure Turbine, Bypass Transition, Separation Bubble

Introduction

In modern high bypass turbofan engines the low-pressure turbine (LPT) has to provide very high power output to drive the fan and additional booster stages very efficiently. As a result, the LPT is one of the heaviest parts of the engine contributing around 1/3 of its overall weight. The current design trend is therefore oriented toward decreasing the number of blades in LPT in order to save weight and secure lower manufacturing and maintenance costs. This implies an increase of the aerodynamic load on each blade. The resulting strong adverse pressure gradient usually induces separation of the suction side boundary layer, particularly under low Reynolds number conditions, which causes a significant loss in engine efficiency [1]. Mayle [1] classified the boundary layer transition on LPT blade into three modes. He considered separated-flow transition mode to be the most important one for LPT. However, boundary layer transition and separation depend strongly on Reynolds number and freestream turbulence and are affecting each other [2,3]. Consequently, understanding the physics behind these processes and developing to predict them is crucial for the development of lighter and more efficient aeroengines.

The objective of this paper is to investigate the influence of Reynolds number and freestream turbulence intensity (FSTI) on the process of boundary layer transition over the suction side of LPT blade. Detailed boundary layer measurements are performed by use of a hot-wire anemometer. This paper mainly focuses on how freestream turbulence affects the transitional behavior of the

Received: September 2011
Hideo Taniguchi: Assistant Professor

the boundary layer before and after the separation.

Experimental Facility and Measurements

Figure 1 shows the test apparatus, showing the test linear cascade and the position of the turbulence grid. The three-blade cascade configuration has been chosen to make each of the blades as large as possible in order to increase the spatial resolution of the measurement. The cascade characteristics are listed in Table 1. The cross-section of the cascade blade is a typical profile of modern commercial aeroengine LPT. Two guide plates, shown in Fig. 1, are needed to produce the correct exit flow angle from the cascade and the pitchwise periodicity.

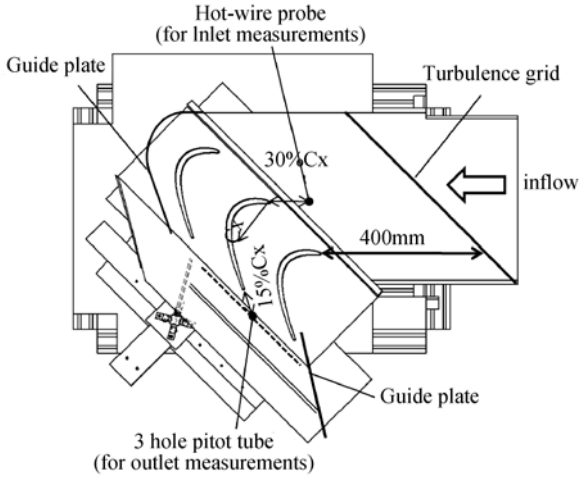

Fig. 1 Experimental apparatus

Table 1 Cascade characteristics

Chord C [mm]	308
Axial chord Cx [mm]	270
Span h [mm]	300
Inlet flow angle β_1 [deg]	45
Exit flow angle β_2 [deg]	60

The measurements were carried out at Re = 130,000, 170,000 and 210,000. The Reynolds number, as defined above, is based on the chord length and averaged exit velocity. The exit velocity distribution was carefully measured, averaged and then adjusted for every test case until the specified averaged exit was obtained. The velocity distribution was measured with a 3-hole pressure probe traversing 15% chord length downstream of the cascade outlet plane.

The inlet freestream turbulence was measured with a single-wire probe positioned 30%Cx upstream of the inlet plane of the cascade. Two types of turbulence grids were placed 400 mm upstream of the inlet plane of the cascade, which are as shown in Figure 1, to enhance inlet freestream turbulence.

A single hot-wire probe (DANTEC 55P11) and a constant temperature anemometer (Kanomax model-1011) were used for the boundary layer measurement over the airfoil suction surface. The probe was traversed using a 2-axis computer-controlled traversing mechanism with a minimum linear translation step of 0.02mm.

Results and Discussion

Figure 2 shows time averaged velocity contours for each FSTI cases at Re=170,000. In these figures dots denote peak positions of RMS velocity fluctuation at each streamwise location. In addition, the time variations of velocity over 0.1 second are plotted for several positions. In this study, judgment about whether boundary layer separation occurs or not was based on overall evaluation by using the information of time averaged velocity, RMS velocity fluctuation, power spectrum of velocity fluctuation, shape factor and so on. The separation location was identified as the one at which the spatial growth rates of time averaged velocity and RMS velocity fluctuation at the measurement point closest to the wall turned from positive to negative. The separation location was found to be about 69% Cx for the range of Reynolds numbers and inlet FSTI adopted in the present study, and don't depend strongly on the Reynolds number or FSTI. The separation occurred in the case of Tu = 0.5% and 4.5%, and was not observed clearly in Tu = 6.1% case. The velocity time traces of Fig. 2(a) show that periodic small-amplitude fluctuation began to appear near the separation location, growing into harmonic disturbances, ending up with transition to turbulence. On the other hand, Figs. 2(b) and 2(c) show that high-amplitude fluctuations already appeared at 60% Cx, excitation of harmonic disturbances and transition arise for relatively short distance.

Figure 3 shows RMS velocity fluctuation contours for each FSTI cases at Re=170,000. The reattachment location is identified as the one at which both of time averaged velocity and RMS velocity fluctuation near wall begin to rise sharply downstream of separate location. The reattachments occur at around 78～80% Cx for the case of Tu = 0.5%, and at around 75～76% Cx for the case of Tu = 4.5%. In the case of Tu = 0.5%, the velocity fluctuation was observed to develop slowly in the separated shear layer. But strong turbulence emerged and spread rapidly normal to the wall after reattachment. In the case of Tu = 4.5%, the velocity fluctuation was observed to develop from the leading edge, while the region of high turbulence appeared after reattachment. In the case of Tu = 6.1%, the intense velocity fluctuation was observed upstream, the region of rising turbulence appearing around 70% Cx without clear indication of separation.

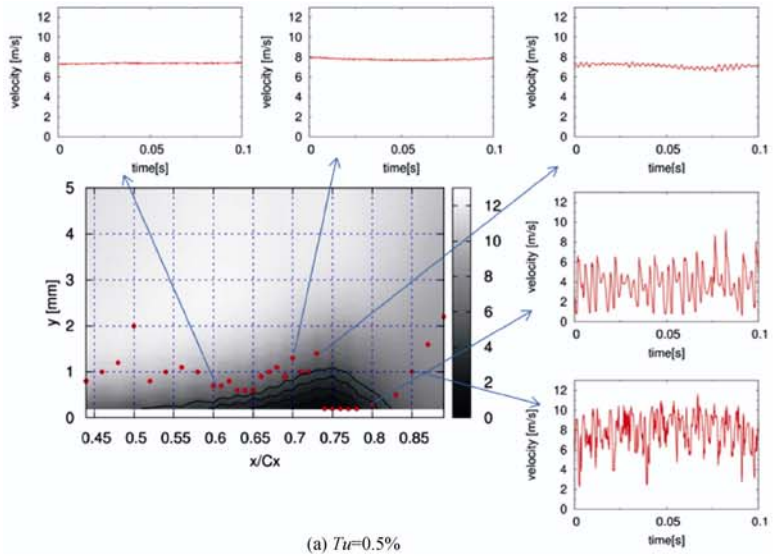

(a) *Tu*=0.5%

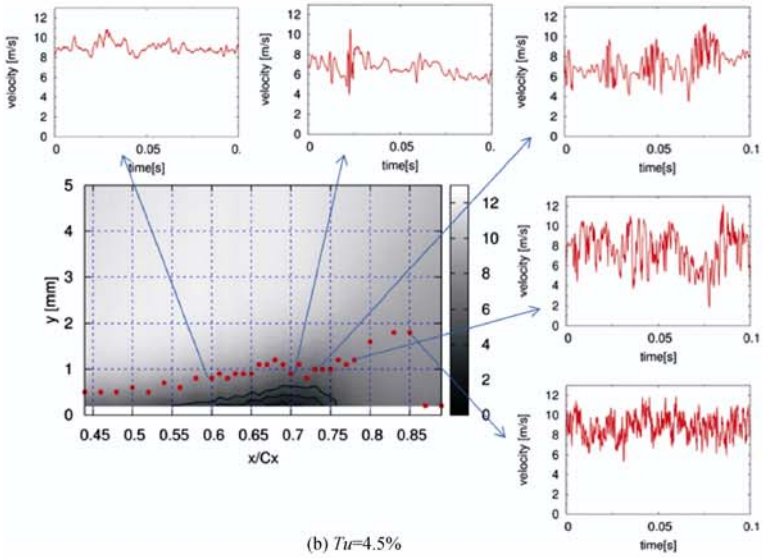

(b) *Tu*=4.5%

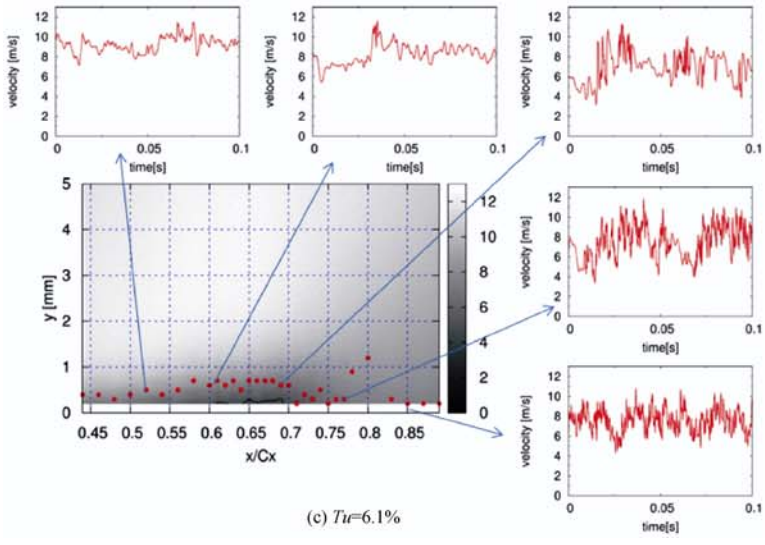

(c) *Tu*=6.1%

Fig. 2 Time-averaged velocity contours (*Re*=170,000)

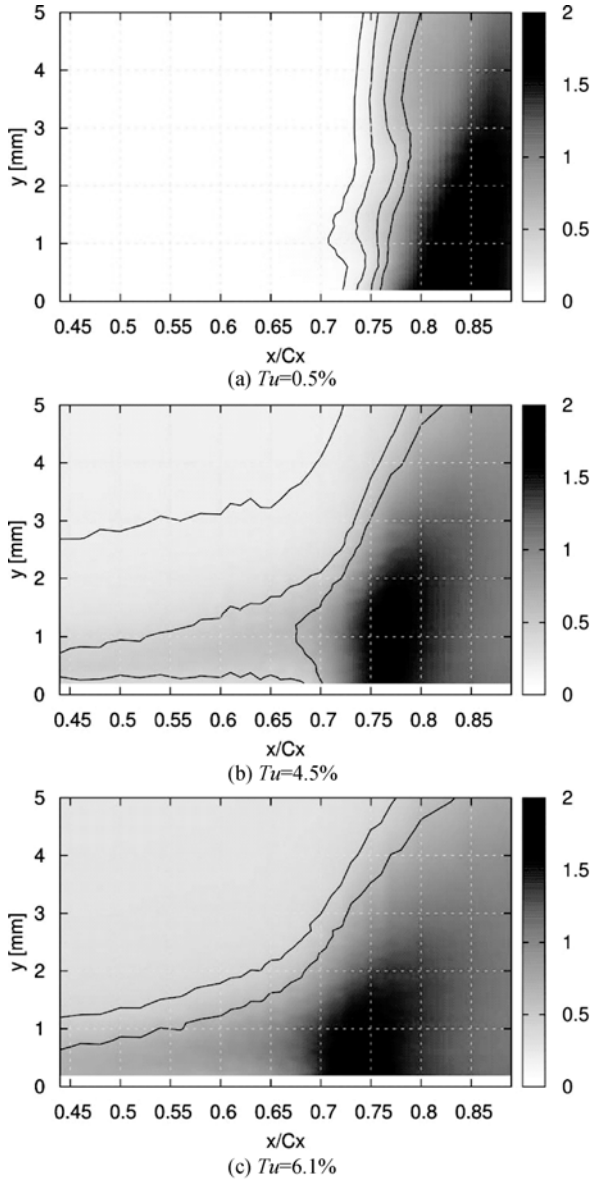

Fig. 3 RMS velocity fluctuation contours (*Re*=170,000)

Figure 4 shows power spectra of velocity fluctuation for each FSTI cases at *Re*=170,000. These figures represent the results of FFT analysis of the velocity data acquired at the dots as shown in Figure 2. In order to analyze spectrum peaks, frequencies of Tollmien- Schlichting (T-S) wave and Kelvin-Helmholtz (K-H) instability were calculated in the same manner as Chandrasekhar[4] and Walker[5]. Figures 4(a) and 4(b) show that there are spectrum peaks near 300Hz. These peaks were found to be that of K-H instability by estimation, as mentioned above. Figure 4(c) show that there is no distinct spectrum peaks. This indicates that velocity fluctuations with broad frequency band are introduced in the boundary layer, they grow up downstream and lead to transition. In Fig. 4(a), there are some spectral peaks in the frequency range from 80 to 250Hz with the peak near 300Hz. The peak near 180Hz seems to be that of T-S wave because the frequency of T-S wave is estimated to be 187Hz through the correlation of Walker[5]. At present, we have no idea what phenomenon induced the other peaks in Fig. 4(a).

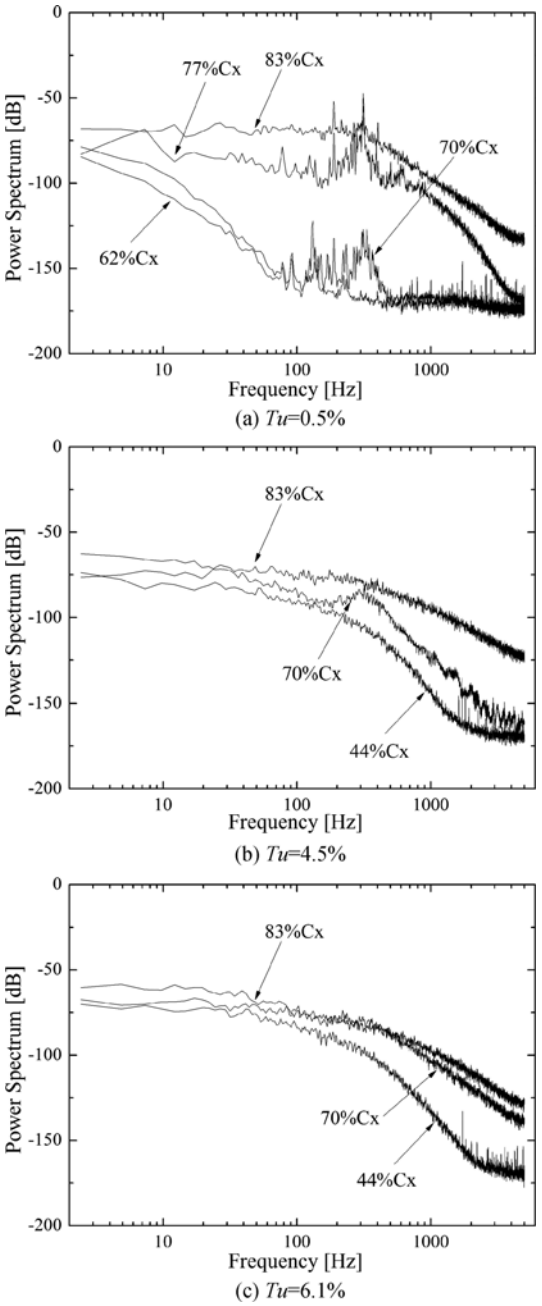

Fig. 4 Power spectra of velocity fluctuation (*Re*=170,000)

Figure 5 shows RMS velocity fluctuation profiles for each FSTI cases at *Re*=170,000. The abscissa of this plot is RMS value normalized with local edge velocity, while the ordinate of this plot is the distance from the wall normalized with local displacement thickness. In the case of *Tu* = 4.5% and 6.1%, there are typical profiles having

peaks near y/δ*=1.3 and slow amplitude decay with distance normal to the wall, except profile of 70% Cx. These profiles indicate that there are the streamwise streak structures, also called Klebanoff mode, in the boundary layer. The growth of near-wall streaks is a key phenomenon triggering the bypass transition leading to breakdown and turbulence production. The profiles of 70% Cx in Figs 5(a) and 5(b) are that of K-H instability because separation locations for both cases are near 69% Cx. The profile of 70% Cx in Fig 5(c) presents a typical one of attached boundary layer.

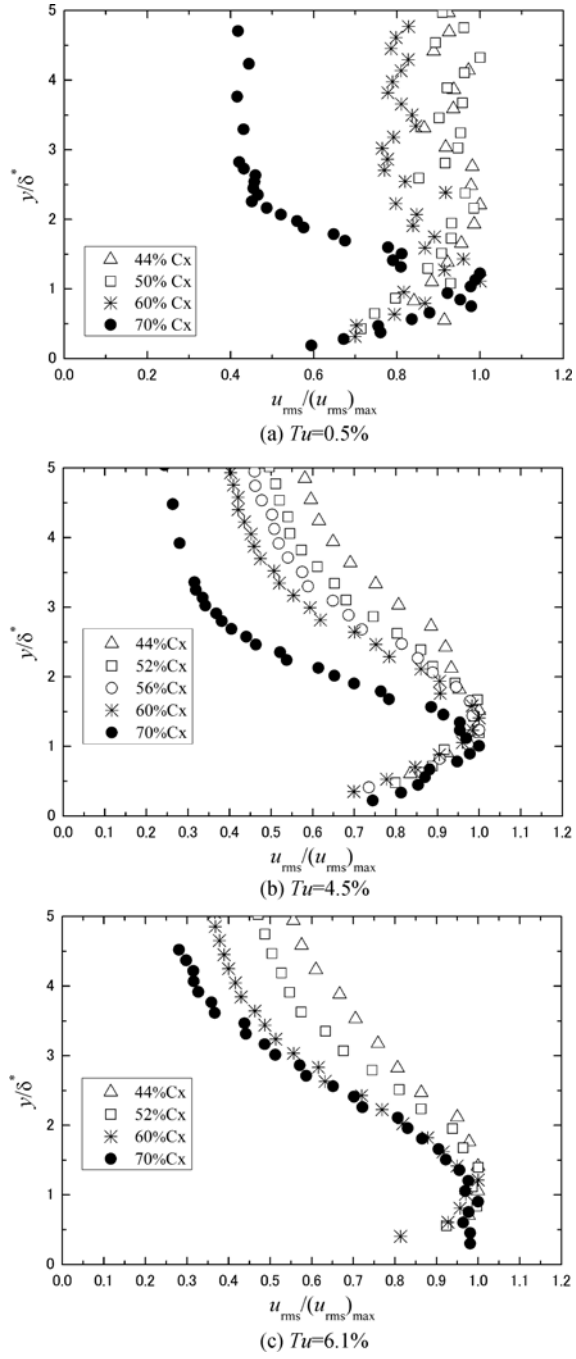

Fig. 5 RMS velocity fluctuation profiles (*Re*=170,000)

Figure 6 shows intermittency factor distributions for each FSTI at *Re*=170,000. Those plots are the peak intermittency at each streamwise location. The intermittency was calculated as follows,

$$\gamma(x) = \frac{1}{N}\sum_{k=1}^{N} I_k(x,t) \tag{1}$$

$$I_k(x,t) = \begin{cases} 1 & \text{when} \quad D(t) \geq C_{tr} \\ 0 & \text{when} \quad D(t) < C_{tr} \end{cases} \tag{2}$$

where the turbulence detector function $D(t)$ defined by

$$D(t) = \frac{(\Delta u/\Delta t)_{\mathrm{RMS}}}{U_e^2/\delta} \tag{3}$$

was used. $D(t)$ is based on a window averaged value of $(\Delta u/\Delta t)_{\mathrm{RMS}}$, local boundary layer edge velocity U_e and local boundary layer thickness δ. The timescale t_s, the window period t_w and the non-dimensional window period C_{wp} are defined as

$$t_s = \delta/U_e, \quad C_{wp} = t_w/t_s \tag{4}$$

The values of C_{tr} and C_{wp} were chosen in a trial-and-error manner. The value of N was more than 2000 although N varied with C_{wp}. In this study, the onset of transition was defined as the location of γ= 0.1. The onsets of transition occur at about 79–80% Cx for the case of *Tu* = 0.5%, about 71–72% Cx for *Tu* = 4.5% case, and about 68%–69% Cx for *Tu* = 6.1% case. The intermittency of *Tu* = 6.1% indicates that transition has begun near the separation location of *Tu* = 0.5% and 4.5% cases. For this reason, bypass transition of attached boundary layer seemed to occur without separation in the case of *Re* = 170,000 and *Tu* = 6.1%.

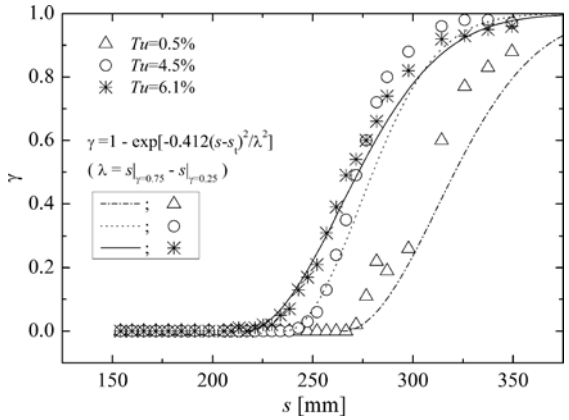

Fig. 6 Distribution of intermittency (*Re*=170,000)

Figure 7 shows time averaged velocity contours at *Re*=170,000 and 210,000 for *Tu* = 0.5% case. These figures present that the size of separation bubble decreases as Reynolds number increases. In general, with the increase of Reynolds number, the boundary layer thickness becomes thin, the growth rate of turbulence is elevated

and the reattachment of separated shear layer is promoted. The results of Fig. 7 and Fig. 8 are consistent with this.

Figure 8 shows the squared value of maximum RMS velocity fluctuation for the downstream location. This figure presents that the growth rate of turbulence varies according to Reynolds number and FSTI.

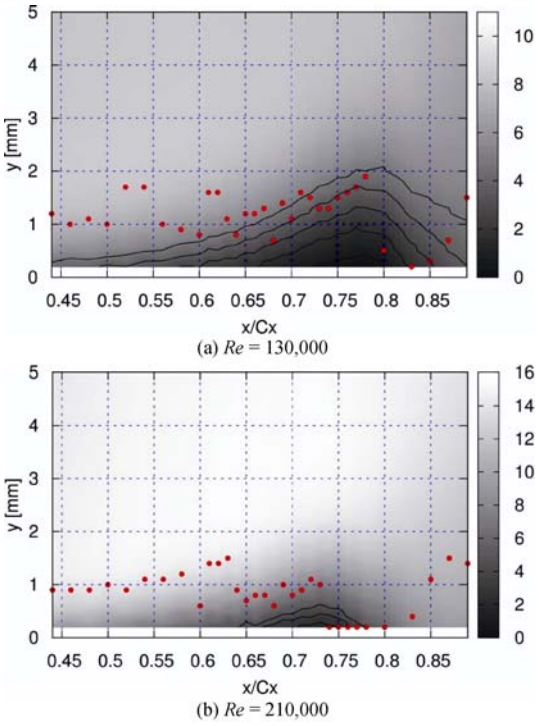

Fig. 7 Time-averaged velocity contours (Tu = 0.5%)

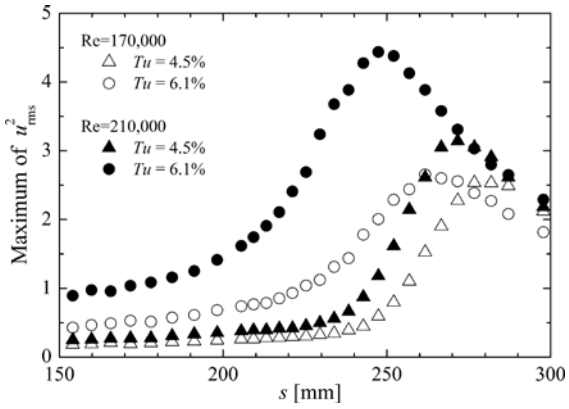

Fig. 8 Distributions of maximum $(u_{rms})^2$

Conclusion

The influence of Reynolds number and freestream turbulence intensity on the process of boundary layer transition over the suction side of Low-pressure Turbine blade has been studied experimentally. The location of boundary layer separation does not strongly depend on the freestream turbulence level and Reynolds number. As the freestream turbulence level increases, the size of separation bubble becomes small and the location of turbulent transition moves upstream. The size of separation bubble becomes small as the Reynolds number increases. At low freestream turbulence intensity, the velocity fluctuation due to Kelvin-Helmholtz instability is observed clearly in the shear layer of the separation bubble. At high freestream turbulence intensity, the streak structures appear upstream of the separation location, indicating bypass transition of attached boundary layer occurs at high Reynolds number.

References

[1] Mayle, R. E.: The Role of Laminar-Turbulent Transition in Gas Turbine Engines, ASME J. of Turbomachinery, Vol.113, pp.509–537, (1991).

[2] Huang, J., Corke, T. C., and Thomas, F. O.: Plasma Actuators for Separation Control of Low-Pressure Turbine Blades, AIAA Paper 2003-1027, Reno, Nevada..

[3] Volino, R. J., Hultgren L. S.: Measurements in Separated and Transitional Boundary Layers Under Low-Pressure Turbine Airfoil Conditions, ASME J. of Turbomachinery, Vol.123, pp.189–197, (2001).

[4] Chandrasekhar, S.: Hydrodynamic and Hydromagnetic Stability, Clarendon Press, Oxford, (1961).

[5] Walker, G., J.: Transitional Flow on Axial Turbomachine Blading, AIAA J., Vol.27, pp.595–602, (1989).